Ultracompact Superconducting Isochronous Cyclotron Production of ^{13}N for Positron Emission Tomography Applications

By

Shawn Fitzgerald

B.S. Chemistry and Chemical Engineering

United States Military Academy, 2003

SUBMITTED TO THE DEPARTMENT OF NUCLEAR SCIENCE AND ENGINEERING IN PARTIAL FULFILLMENT OF THE REQUIREMENTS FOR THE DEGREE OF

MASTER OF SCIENCE IN NUCLEAR SCIENCE AND ENGINEERING AT THE MASSACHUSETTS INSTITUTE OF TECHNOLOGY

JUNE 2013

Signature of Author: _____
Shawn Fitzgerald
Department of Nuclear Science and Engineering

Certified by: _____
Richard C. Lanza
Senior Research Scientist
Thesis Supervisor

Certified by: _____
Benoit Forget
Assistant Professor of Nuclear Science and Engineering
Thesis Reader

Accepted by: _____
Mujid S. Kazimi
TEPCO Professor of Nuclear Engineering
Chair, Department Committee on Graduate Students

Ultracompact Superconducting Isochronous Cyclotron Production of ^{13}N for Positron Emission Tomography Applications

By

Shawn Fitzgerald

Submitted to the Department of Nuclear Science and Engineering on May 6, 2013 in Partial Fulfillment of the Requirements for the Degree of Master of Science in Nuclear Science and Engineering

ABSTRACT

Testing was performed on a data acquisition (DAQ) system that was built specifically to characterize a new ultracompact superconducting isochronous cyclotron (USIC) at MIT. A production model of Nitrogen-13 was validated by experiment at Massachusetts General Hospital. Both absolute and relative activity calculations were conducted utilizing an original MATLAB script; it is demonstrated that relative activity calculations are both more accurate and precise. The DAQ system limitations in terms of potential activity calculations were also explored. A saturation limit of 3500 coincident counts per second was calculated and validated, which sets a design criterion limit for future work. The potential for the USIC to be utilized in an active SNM interrogation role is also explored.

Thesis Supervisor: Richard C. Lanza
Title: Senior Research Scientist, Department of Nuclear Science and Engineering

Acknowledgements

This thesis represents the culmination not only of many months of thought and writing, and many hours of work both in the NW13 vault and the MGH "hot cell." And for that, there are many people to thank.

First and foremost, my family. Thank you for your unending and continued support.

The faculty and staff within the Nuclear Science and Engineering Department. I've learned so, so much over the past two years from people like Richard Lester, Bilge Yildiz, Benoit Forget, Jackie Yanch, Mike Hynes, and Paola Cappellaro.

To my thesis advisor, Dick Lanza, a very special thank you. I appreciate all the help and support both in this project. I was hoping that this thesis would test and characterize the USIC, but I appreciate the flexibility granted by you to work on the DAQ system. I've learned more than I ever cared to know about NaI crystals and LINUX operating systems.

The faculty and staff within the Political Science Department, for the understanding, freedom, and permission in allowing me to pursue dual masters degrees.

To my fellow graduate students, thank you for supporting me and helping me out through the tough classes and the tougher skits. It's impossible to name you all, but Mark Reed, Nathan Gibson, Will Boyd, Lulu Li, Rosie Sugrue, Brittany Guyer, Sara Ferry, David Bloore, Becky Romatowski, Mohit Singh, and Ty Sordelet have been especially awesome.

To my real partners in crime, Mareena Robinson, Chad Schools (sir), Buck O'Day (sir), you guys have been amazing over the past couple of years. I wish you the best in completing your studies at MIT.

To Zach Hartwig, I sincerely appreciate all the personal support on this project. While I realize that this masters thesis would make up a small portion of one of the chapters of your dissertation, I thank you for the patience and for teaching me more about "real" nuclear engineering than I learned in some entire classes.

To the folks at Massachusetts General Hospital – Georges El Fakhri and especially Dave Lee, Jack Correia, and Ron Moore – I really appreciate the support and the "custom" cyclotron runs you allowed me to perform. I wasn't kidding, I do owe you each a 6-pack of Sam Adams.

To MIT; thank you for allowing me two amazing years here, and while I'm leaving with slightly less hair than I came with, I'm leaving with much more knowledge than I ever thought possible.

TABLE OF CONTENTS

INTRODUCTION

Positron Emission Tomography (PET) is a nuclear medicine imaging technique used to map biological processes in the human body. In this procedure, a biological compound is "labeled" with a radionuclide and then administered to a patient. The radiopharmaceutical is distributed throughout the body and accumulates within an organ of interest. The labeled radionuclide then decays via positron emission within that organ. The positron interacts with, and annihilates, neighboring electrons, producing dual 511-keV gammas in opposite directions, or lines of coincidence (LOCs). The PET scanner, consisting of a scintillator and a photomultiplier, can pinpoint the location of the annihilation event based simply on the geometry of the LOCs. This response is used to create a three-dimensional image of the biological process of interest. This image can be paired with a normal magnetic resonance imaging (MRI) or computed tomography (CT) image to provide both structural and metabolic information about the organ of importance.

A variety of radionuclides may be used in the PET technique, most notably ^{11}C ($T_{1/2}$ = 20 min), ^{13}N (10 min), ^{15}O (2 min), and ^{18}F (110 min). These may be utilized in different sets of radiopharmaceuticals in order to map different metabolic processes. For example, glucose labeled with ^{11}C can provide information on glucose utilization, and ^{15}O may provide data on blood volume. Radiolabeled ammonia, $^{13}NH_3$, can be used to measure blood flow, which is useful in diagnosing diseases in the heart.[1] These radioisotopes are most often produced in a cyclotron. Due to their short half-lives, the

cyclotron facility must be located in close proximity to both the chemical lab that produces the radiopharmaceutical and the imaging clinic. These facilities must maximize safety considerations and minimize the radiation dose received by both the patient and the hospital workers.

Normally, the cyclotron facilities are large and expensive to maintain. A less expensive, smaller cyclotron may provide a more affordable method of producing radioisotopes, radiopharmaceuticals, and ultimately, providing PET imaging capability, as well as access to shorter-lived isotopes, to hospitals not otherwise able to afford it.

IONETIX has developed an ultracompact superconducting isochronous cyclotron (USIC) that would meet the specifications required in a clinical setting, but this new machine has not yet been tested. As part of initial testing, a detection and data acquisition (DAQ) system must be built, tested, and characterized. This thesis work will embark on the following objectives:

First, I will provide a brief overview of the history and basic physics involved in the cyclotron, paying special attention to the characteristics of a compact superconducting isochronous cyclotron. This will be useful in describing why the IONETIX design is optimal for PET and other mobile/remote applications. Second, I will review existing literature describing the ^{16}O (p,α) ^{13}N reaction. This is important because it will provide the scientific basis for the results that I expect to see in my experiment. Third, I will describe the setup and design of my experiments that will characterize the USIC's DAQ

system. Next, I will present our data and results from these first experiments. Fourth, I will describe the ^{11}B (d,nγ) ^{12}C reaction, another potential application of a mobile cyclotron and one that is useful for active interrogation of special nuclear material (SNM). Fifth, I will utilize my initial DAQ testing results to comment on future experiment design. Lastly, I will comment on general improvements that might be made to the DAQ system and what effect those improvements would have on the ability to conduct activity measurements.

This thesis work makes two important contributions. First, it will optimize the experimental design for the DAQ system given USIC operational parameters. This will allow for eventual proof of concept of the cyclotron's ability to produce radionuclides for PET imaging. Second, this thesis work will demonstrate the potential utility for the USIC DAQ system to measure gamma production that might be used for national security applications.

Cyclotron Fundamentals

Any discussion of cyclotron physics must start with the basic equation for force that an ion sees in the cyclotron. A charge sees a centripetal force in a magnetic field according to Equation 1.1:

$$\frac{Mv^2}{r}\hat{r} = q\vec{v}\times\vec{B} \qquad (1.1)$$

where M is the mass of the ion, v is its velocity, r is the radius of motion, q is the charge, and B is the magnetic field.

If we choose an axial magnetic field B and an azimuthal velocity v, the equation becomes:

$$\frac{Mv^2}{r} = qvB \tag{1.2}$$

There are two interesting quantities that are seen in this equation. The first is that the radius of a cyclotron is governed by the relation:

$$r = \frac{Mv}{qB} \tag{1.3}$$

Specifically, as the magnetic field of the cyclotron increases, the radius decreases. The second interesting characteristic that comes from Equation 1.2 is the cyclotron period (and the related quantity of the cyclotron's frequency). Rearranging Equation 1.2, we obtain:

$$\omega_0 = \frac{v}{r} = qB / M \tag{1.4}$$

where ω_0 is the cyclotron's period. The cyclotron's frequency is related to the period by:

$$f_0 = \frac{\omega_0}{2\pi} \tag{1.5}$$

It is important to keep in mind that as ion speed approaches relativistic speeds, the equations above are modified according to the equations below, where $\gamma = \frac{1}{\sqrt{1-\frac{v^2}{c^2}}}$ and c is the speed of light :

$$M = \gamma M_0 \tag{1.6}$$

$$\omega = \gamma \omega_0 \tag{1.7}$$

$$f = \gamma f_0 \tag{1.8}$$

Thus, for a cyclotron in which the ions increase in velocity as they increase in radial path, we need a way to account for relativistic effects. There are three basic cyclotron designs that account for these relativistic effects differently.

The original cyclotron design pioneered by Lawrence in 1931 simply ignored relativistic effects and mass increases, operating at a fixed frequency. A major consequence of this design failure is that as the ions increase in mass, the ion period ω_0 begins to fall behind the RF period, and the ions do not cross the gaps at the correct time intervals. Eventually, the ions will begin to cross the gaps when the voltage has the wrong sign and will decelerate. In order to maximize ion energy with this design, the

ions must be extracted from the cyclotron before deceleration begins.[2]

A cyclotron design that handles the relativity effects is the synchrocyclotron. In this machine, the RF frequency decreases as the ion energy and mass increase. In mathematical terms, the synchrocyclotron frequency is "matched" and synchronized with the relativistic mass increase during acceleration, according to Equation 1.10.

$$\omega_{RF} = \frac{\omega_0}{\gamma} = \frac{qB}{\gamma M_0} \tag{1.10}$$

The isochronous cyclotron approaches the relativity problem differently. Instead of varying the RF frequency (which requires a very complex RF system), the isochronous design results in increased magnetic field strength B with increasing radius. If we increase the magnetic field according to the relativistic factor γ, we recognize that the cyclotron's RF frequency and period remain constant:

$$\omega = \frac{qB}{M} = \frac{q\gamma B_0}{\gamma M_0} = \frac{qB_0}{M_0} \tag{1.11}$$

The fixed RF frequency eliminates the issues with the RF system design with a synchrocyclotron, but in an isochronous cyclotron, the magnets must be designed to increase in magnetic field in a way that precisely matches the increased ion mass due to relativity.[3]

In work previously done at MIT, it is noted that the IONETIX superconducting cyclotron design is novel for three reasons. First, the magnets are formed by superconducting niobium titanium coils that will produce a magnetic field of 6 T. This allows USIC to be built with a system diameter of less than 1 m, as compared to a conventional machine such as IBA's Cyclone design, whose radius is 3.66 m.[4] It should be noted that increasing the magnetic field B reduces the diameter by a factor of $\frac{1}{B^2}$ and the height by a factor of $\frac{1}{B}$, therefore reducing the overall volumetric footprint of the cyclotron by a factor of $\frac{1}{B^3}$. Also, since the USIC has superconducting magnets and an isochronous magnetic field, it allows us to produce ion beams at energies with less input power. USIC is designed to run off 220 V / 30 A "wall power."[5] Therefore, the USIC is extremely mobile and can be operated in austere environments where the infrastructure to run an IBA or General Electric design may not be feasible.

Two potentially powerful applications of the USIC design arise out of its mobility. First, the USIC is ideally suited for the production of Nitrogen-13 and other short-lived radionuclides. Whereas Fluroine-18 has a half-life of approximately 110 minutes and can be purchased from a remote production facility for use inside a hospital setting, Nitrogen-13, with a half-life of 9.98 minutes, must be produced in short proximity to the clinic in which it will be used. The use of the USIC can bring PET diagnostic tools to doctors in remote hospitals or hospitals without the infrastructure to support a large cyclotron. The main work of this thesis will be to characterize the detection and data acquisition system that will prove USIC's utility with regard to radionuclide production. Second, the

USIC's mobility allows it to be positioned in locations that require high-energy gamma production for active interrogation of SNM. The USIC would be a component of a detection system that would utilize photofission signatures of fissile material in order to screen cargo. Additionally, the USIC could be used as a part of a transmission radiography system. Many locations, such as border crossings, ports, and airports would not have requisite infrastructure to support a large cyclotron as a part of this detection system. However, since the USIC can run off "wall" or generator power, it could provide policymakers and government officials additional options with regard to assets at US and international ports of entry. The secondary objective of this thesis is to provide some experimental parameters that will allow for characterization of the USIC's ability to produce high-energy gammas necessary for this detection scheme.

Now that I have provided some background in terms of the motivation and general strategy for this thesis work, I will now review the science of Nitrogen-13 production. This will lay groundwork for the experimental design and code required to analyze experimental results.

PET IMAGING: THE ^{16}O (p,α) ^{13}N REACTION

The nuclear reaction to produce Nitrogen-13 has become popular in recent years due to the radioisotope's ability to "tag" ammonia in order to image cardiologic processes with PET.

Kumar et. al describe three separate reactions to form Nitrogen-13: alpha particle irradiation of boron nitride in sodium hydroxide; deuteron irradiation of methane gas or metal carbides; and proton irradiation of natural water.[6] The ^{16}O (p,α) ^{13}N reaction is the most efficient in terms of production yield. Yield of Nitrogen-13 tagged ammonia is further enhanced by the presence of ethanol in the natural water target, which inhibits the formation of other nitrogen-containing compounds.[7] According to the IAEA, proton bombardment of water results in nitrates and nitrites, which must be reduced by de Varda's alloy in order to produce ammonia. However, ammonia can be produced in the water target directly with the presence of a reducing agent or a radical inhibitor.[8]

Reaction Characteristics

The proton ion beam reaction to produce Nitrogen-13 can be written as:

$$^{16}_{8}O + ^{1}_{1}H \rightarrow ^{13}_{7}N + ^{4}_{2}\alpha$$

In order to determine anticipated production rates from a proton beam, we must examine the excitation function of the reaction. The IAEA NDS examined ten experiments and provides a calculated cross-section fit based on experimental data.

Figures depicting the experimental data and the curve fit appear below. For 11 MeV protons (the USIC's designed proton beam energy), the IAEA recommends using a cross-section of 45.5 millibarns.[9]

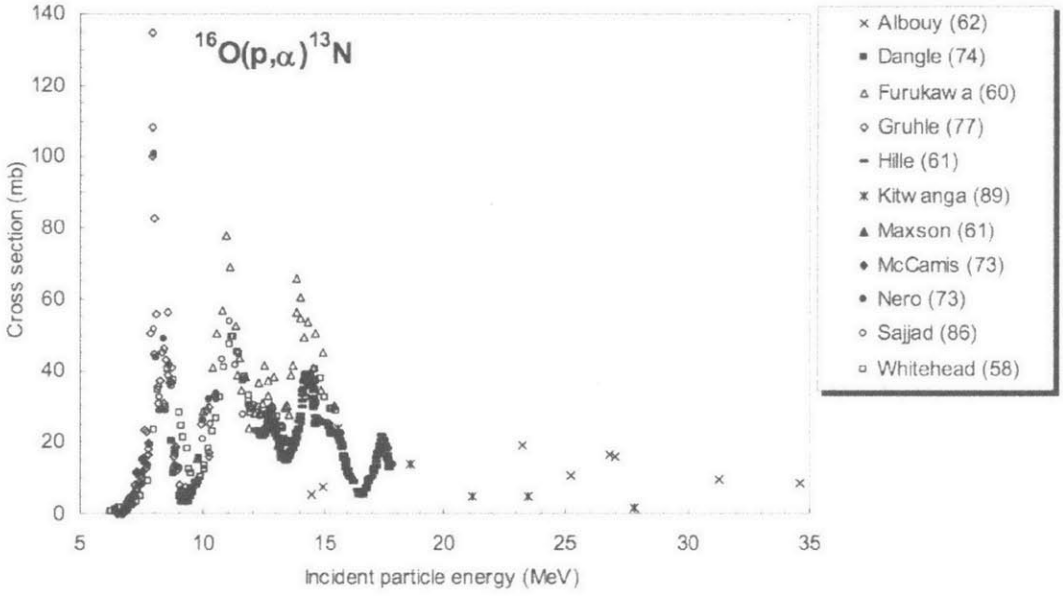

Figure 2.1: All IAEA Experimental Data.[10]

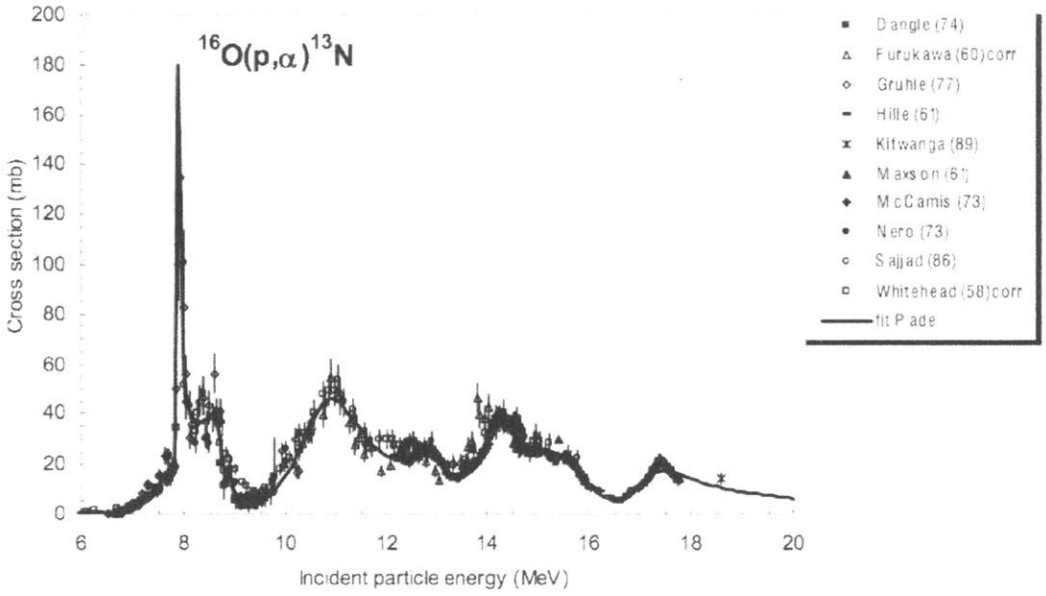

Figure 2.2: Experimental Data with Recommended Cross-Section Curve.[11]

Once the Nitrogen-13 is formed, it decays by positron emission (100%) with a half-life of 9.98 minutes. The positron annihilates with nearby electrons, resulting in dual 511-keV gamma rays emitted at 180 degrees to each other. This allows the PET scanning equipment to locate and map the location of the Nitrogen-13, and, in essence, the blood and tissue that carries the tagged ammonia. This characteristic will also aid in my experimental design, as I will detect and count 511-keV gammas.

Production Rate of Nitrogen-13

The standard production rate model for any radionuclide from beam irradiation is described by Choppin, Liljenzin, and Rydberg (2002) using target geometry and reaction cross-section.

For the general case, we examine the reaction:

$$X_{tgt} + X_{proj} \xrightarrow{k} X_1 \xrightarrow{\lambda_1} X_2 \tag{2.1}$$

For our particular reaction of interest, we have:

$$^{16}O + p \xrightarrow{k} {}^{13}N \xrightarrow{\lambda_{13}} {}^{13}C + \beta^+ (2 \times 511\ keV\ \gamma) \tag{2.2}$$

For Nitrogen-13 specifically, we have:

$$t_{1/2} = 9.98\ \text{min} = 598.8\ \text{sec} \tag{2.3}$$

$$\lambda_{13} = \frac{\ln 2}{t_{1/2}} \tag{2.4}$$

The production of Nitrogen-13 by an irradiating beam is given by the differential equation:

$$dN = k\ dt - \lambda_{13} N\ dt \tag{2.5}$$

Where N is the number of Nitrogen-13 atoms and k is the production rate in units of atoms per second. Integrating this equation from time $t = 0$ to some future time of irradiation, and assuming no Nitrogen-13 exists at time $t = 0$, we have:

$$N = \left(\frac{k}{\lambda_{13}}\right)\left(1 - e^{-\lambda_{13} t_{irr}}\right) \tag{2.6}$$

Equation 2.6 is a function of the beam irradiation time; this equation gives the number of Nitrogen-13 atoms present during beam irradiation. The "cooldown" equation after irradiation is given by:

$$N = \left(\frac{k}{\lambda_{13}}\right)\left(1 - e^{-\lambda_{13} t_{irr}}\right)\left(e^{-\lambda_{13} t_{cool}}\right) \tag{2.7}$$

where $t_{cool} = t - t_{irr}$. We can rewrite the above equations in terms of activity (a measurable quantity). Remembering:

$$A = \frac{\Delta N}{\Delta t} = \lambda_{13} N \tag{2.8}$$

we obtain:

$$A = k\left(1 - e^{-\lambda_{13} t_{irr}}\right)\left(e^{-\lambda_{13} t_{cool}}\right) \tag{2.9}$$

The production rate for this particular reaction, k, is given by the equation:

$$k = 6.24 \times 10^{18} I \sigma N_v x \tag{2.10}$$

where I is the beam current in amps, σ is the reaction cross section in cm^2, N_v is the

number of target atoms per unit volume (in cm^3), and x is the beam stopping power in the target (cm). The quantity $N_v x$ gives the number of target atoms per unit area (cm^{-2}). The constant 6.24×10^{18} comes from the definition of one amp (one amp = 6.24×10^{18} protons per second). It should be noted that the constant here would differ for a deuteron beam.

An alternate model is based on the saturation yield of the target material at a given current and energy. This is the method utilized by Eric Marshall in his 2012 thesis describing the preliminary investigation of this reaction. The model proceeds as follows:

For a given beam current, we can expect a yield of a radionuclide due to its saturation yield. According to the IAEA, this saturation yield follows the curve in Figure 2.3.

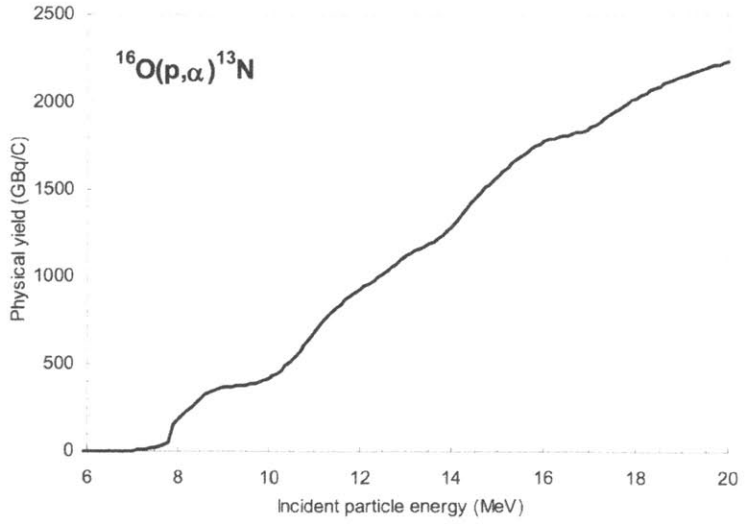

Figure 2.3: Yield of ^{13}N from the recommended cross-sections.[12]

For 11 MeV protons, we expect a physical yield of 675 GBq/C (gigaBecquerel per Coulomb). In order to calculate the production rate (or, more accurately, the activity due to the production of the radionuclide) within the target during irradiation, we use the equation:

$$A_{13} = A_{s13}\left(1 - e^{-\lambda_{13} t_{irr}}\right) \tag{2.11}$$

In order to calculate the activity due to the decay of the radionuclide after irradiation, we use the equation:

$$A_{13} = A_{s13}\left(1 - e^{-\lambda_{13} t_{irr}}\right)\left(e^{-\lambda_{13} t_{cool}}\right) \tag{2.12}$$

For the purposes of this thesis, I will utilize the production rate model given by Choppin et. al, since it takes into account geometry and density of the target material.

At this point, I will describe my experimental design and setup.

EXPERIMENT DESIGN

I designed a series of experiments in order to test the DAQ system, which has detectors and both hardware and software components.

For my set of experiments, I used 4" x 4" x 4" Saint Gobain sodium iodide (NaI) scintillation detectors coupled with an HTV R1911 photomultiplier tube. These detectors originally shipped to MIT in November 1986. These detectors are ideal for low-energy gamma detection, as they have high intrinsic efficiency at 511 keV.

The DAQ hardware consists of a standard PC with associated components (mouse, keyboard, monitor), a surge protection and battery backup module, and three CAEN boards that perform the data collection functions. The CAEN V1718 USB-VME board controls both the V1720 digitizer VME board, which digitizes analog waveforms for storage and analysis, and a V6534 board that provides high voltage and current in order to power up to six NaI detectors.

The DAQ software, developed and built by MIT's Zach Hartwig, is a Linux-based software tool that provides a graphical user interface (GUI) in order to control both the V1720 and V6534 boards as well as perform various experimental procedures, such as supplying power to the detectors, calibrating detectors according to known check source energy spectra, analyzing both waveforms as well as spectra. The software allows the user flexibility in terms of setting experimental parameters that maximize performance.

The software is built on the ROOT data analysis toolkit as well as custom C++ code that was developed at MIT.

In addition to the DAQ's online analysis tools, I developed my own MATLAB code in order to perform both absolute and relative activity calculations. This offline analysis capability provides near real-time activity calculations, which will be of immense importance when performing proof of concept experiments with the USIC.

Since the USIC was still undergoing final engineering and testing throughout the course of this thesis work, characterization of the DAQ was performed at Massachusetts General Hospital (MGH). My experiments proceed along three main lines of effort. First, I attempt to validate the model of Nitrogen-13 production rate. This is important because it will allow IONETIX personnel to adjust beam current and time on target to achieve desired activities when they proceed with their proof of concept experiments. Second, I attempt to comment on error propagation throughout the Nitrogen-13 process. This line of effort is of value because it allows medical personnel to administer a dose from radiopharmaceuticals to patients within prescribed, known limits. Lastly, I attempt to gain some insight into when the DAQ fails as a system. Due to potentially high count rates and limitations of the detectors, the hardware, and the software, I seek to determine the point at which the system becomes saturated and no longer provides accurate readout. This is important when designing future experiments with this particular DAQ system, especially in terms of detector type and geometry.

My work consisted of four experiments, all of which occurred at MGH. MGH utilizes a General Electric PETtrace cyclotron, and operates at a fixed proton energy of approximately 16 MeV. I used a water target for all experiments, as is planned by IONETIX for the USIC. The results from these experiments are presented and explained in the following section of the paper. Only experiments 1 and 2 yielded useful data due to limitations both of the DAQ system as well as MGH's PETtrace cyclotron. These limitations will be discussed in the results section of the paper.

DATA AND RESULTS

Experiment #1

For the first experiment, I utilized the beam "tune up" from MGH's PETtrace cyclotron as my run. This run consisted of 125 seconds of 16 MeV protons on a water target at an integrated current of 0.026 μA. According to the model presented by Equation 2.6, we would expect this run to produce 64 μCi of activity. The irradiated water was flushed into a vial, which was then placed in a holder surrounded by 0.75 inches of lead in order to decrease the overall count rate in the detectors and prevent saturation of the DAQ system. Lead of this thickness provides a transmission rate of 0.269 for 511 keV gammas.

The dual NaI detectors were calibrated using check sources of Cobalt-60 (1170 and 1330 keV gammas), Caesium-137 (which decays via Barium-137m to emit 662 keV gammas), and Sodium-22, which decays via positron emission, resulting in dual 511 keV gammas. The Sodium-22 source was also utilized in order to produce "known" spectra for relative activity calculations and to test coincidence counting in the DAQ system. The calibration curves for both detectors are displayed below. As expected, the curves are linear.

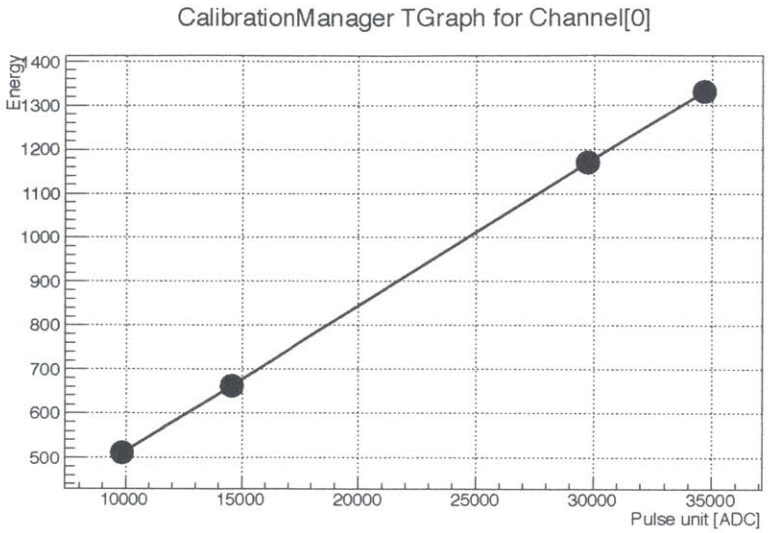

Figure 3.1. Calibration Curve for NaI Detector 1.

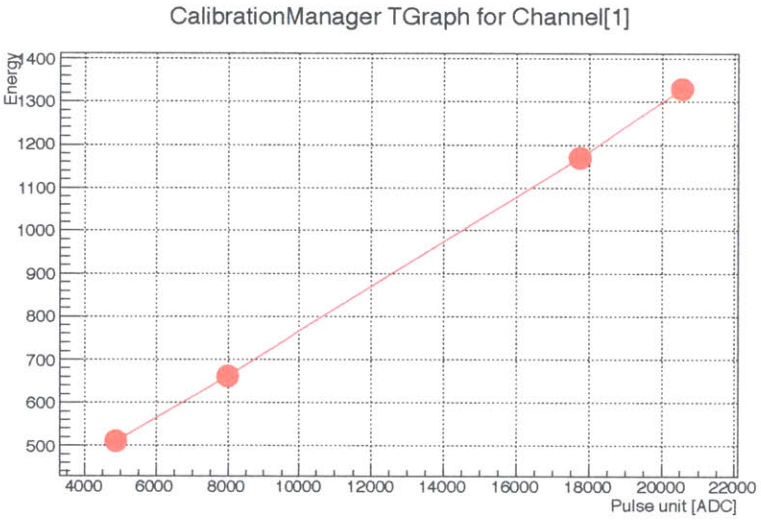

Figure 3.2. Calibration Curve for NaI Detector 2.

Similar linear calibration curves were produced for each experiment, although it should be noted that once calibration is conducted, the user is able to simply input the calibration parameters into the DAQ system for future measurements.

I conducted two types of activity measurements: absolute and relative. In order to calculate absolute activity of a sample, we must take into account the intrinsic efficiency of the detector, the area of the detector, the geometry of the detection scheme, and the collection time. The absolute activity calculation is given by the equation:

$$A = \left(\frac{\Sigma_{13}}{t}\right)\left(\frac{1}{G\varepsilon f}\right) \tag{3.1}$$

where Σ_{13} is the sum of the detector counts due to the decay of Nitrogen-13, t is the collection time (sec), G is the geometric efficiency of the detector scheme, ε is the intrinsic efficiency of the detector for the gamma energy under investigation, and f is the decay fraction of the radioisotope in question. The geometric efficiency G is calculated with Equation 3.2.

$$G = \frac{a}{4\pi s^2} \tag{3.2}$$

Where a is the area of the detector face (cm^2) and s is the source-to-detector distance (cm).

The intrinsic peak efficiency is specified by the manufacturer of the detector, and can be calculated for a given NaI crystal size and gamma energy. Previous work at MIT has resulted in calculation of intrinsic peak efficiency curves for various detector sizes and geometries. The efficiency curves were calculated using GEANT4, and were validated using experimental data.

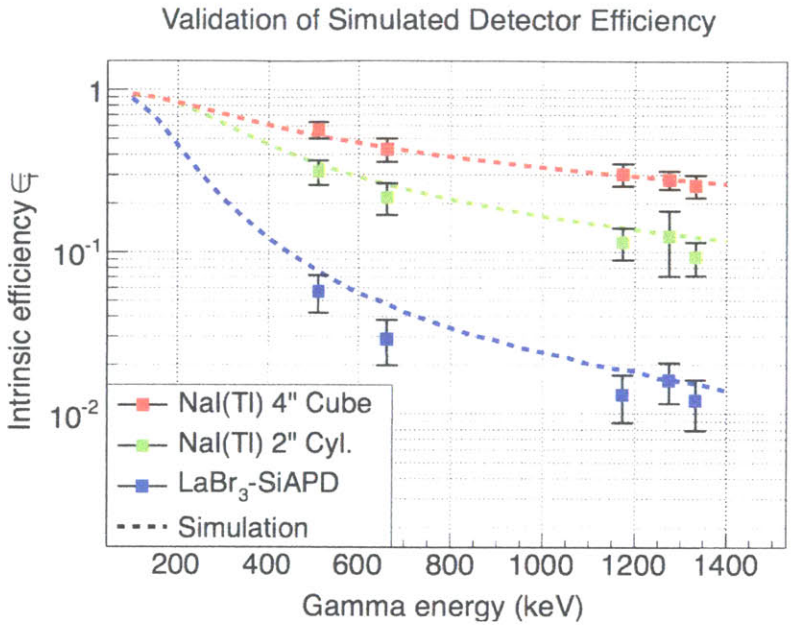

Figure 3.3. Validation of Simulated Detector Efficiency.[13]

For a 4" x 4" x 4" NaI crystal, we take the intrinsic peak efficiency for 511 keV gammas to be 0.44.

The sum of the detector counts, Σ_{13}, in Equation 3.1 is calculated by obtaining two spectra; one "collection spectrum" during an experimental run and subtracting one "background spectrum" with the same collection time.

Alternatively, we can calculate the activity of a sample using the relative method. In this method, a spectrum of a source with an unknown activity is obtained and compared to that of a source with a known activity. This method is presented in Equation 3.3.

$$A = \left(\frac{\Sigma_{13}}{\Sigma_k} \right) A_k \tag{3.3}$$

where Σ_{13} is the sum of detector counts due to Nitrogen-13 decay, Σ_k is the sum of detector counts due to the decay of a source with a known activity and A_k is the activity of the known source. Collection times for the known and unknown acquisitions may vary, as long as those collection times are scaled. This is where the ability to analyze energy spectra offline becomes extremely valuable.

Spectra were saved and collected as .dat text files, and analyzed offline using my MATLAB script, which is included in Appendix 1. Follow-on calculations were conducted using Excel, and the results were plotted, along with corresponding error in each measurement. Error propagation will be explained in the next section of this paper.

The results for the first experiment are displayed in Figure 3.4.

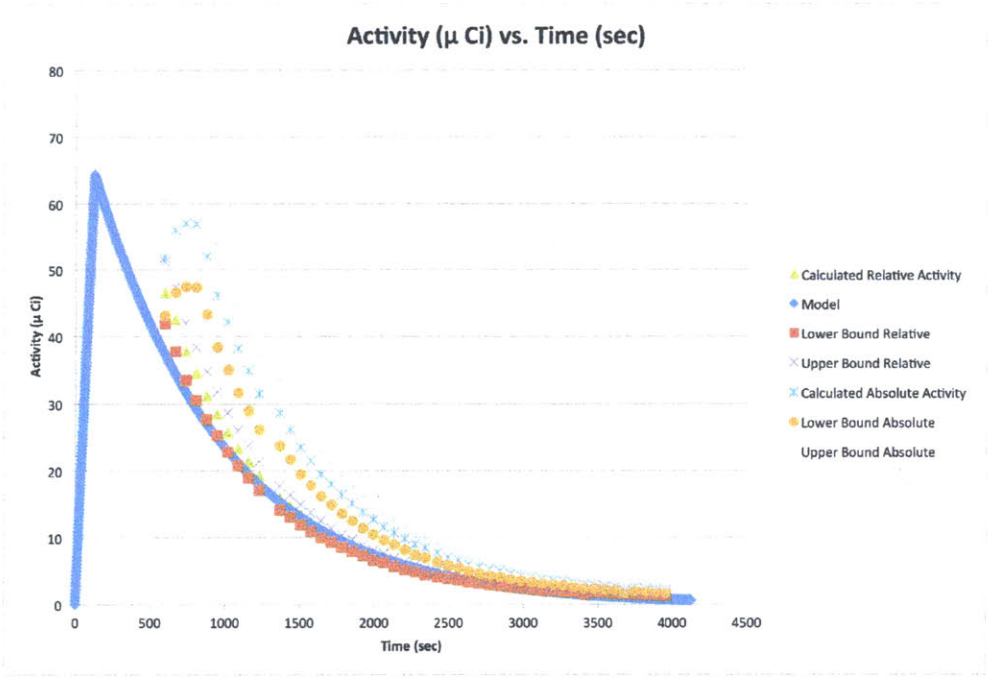

Figure 3.4: Experiment 1 Results.

In general, we see good agreement between the relative activity calculation and what we expect given the production rate model. The results from Experiment 1 show that the relative activity calculation is both more precise and accurate than the absolute activity calculation. There are two related reasons for this. First, utilizing relative activity calculations obviates the need to worry about experimental geometry. As long as the setup of the experiment remains the same, one may conduct multiple acquisitions at multiple activities in order to obtain accurate results. When calculating activity at a given time as in the above figure, we are essentially performing multiple experiments within the same run. Since the activity of the unknown sample of Nitrogen-13 changes with time,

we see the characteristic exponential curve of radioactive decay. The second reason relative calculations are more precise than absolute calculations is that of error propagation. The relative activity calculation contains only three terms with independent error, while the absolute calculation contains five terms with independent error. For this particular experiment, I obtained an error in each relative activity calculation of approximately 11.3%, which the error in each absolute activity calculation was approximately 16.9%. The precision and accuracy of these measurements are of paramount importance when considering patient dose due to a radiopharmaceutical.

Experiment #2

Experiment 2 was conducted using different parameters and with a different intention than Experiment 1. As part of the characterization of the DAQ system, I attempted to calculate the count rate at which the system would become saturated. At the saturation point, the system is not able to register all counts, and is indicated by a red warning light on the V1718 digitizer board. Thus, for a given experimental geometry, there exists an activity above which this detector system cannot provide accurate data.

It should be noted that these calculations were performed using coincidence triggering. That is, the histograms that you see are for one detector (in this case, NaI Detector 1), but events are not plotted to the histogram unless a coincident gamma at the same energy is detected in the second detector. Coincidence triggering ensures that all plots to the histogram arise from positron annihilation events, and not random radiation.

It is likely that the DAQ system's saturation point (in terms of counts per second) for non-coincidence triggering is higher. Since the main purpose of this paper is to characterize the detector system for Nitrogen-13 activity measurements, the non-coincidence saturation point remains outside the scope of this study and was not tested.

Two types of characterization were performed during this experiment. First, I calculated the maximum number of counts that the DAQ could write to the histogram in terms of counts per second while undergoing coincidence triggering and while in "high-rate acquisition" mode. In "high rate acquisition mode" the histogram in the graphical user interface is not continually refreshed, which maximizes possible count rates. This threshold would be useful to future DAQ users when designing experimental geometry. Given a target activity, one could calculate the distance between source and detector necessary to provide accurate counts.

The second goal of this experiment was to assess software performance in terms of histogram refresh rate and its effect on DAQ performance. As part of the graphical user interface, the option exists to refresh a continuously plotted energy spectrum every x events. For this objective, I varied the spectrum refresh rate while the detector was saturated, and calculated the response curve. Figures 3.5-3.7 depict high-rate acquisitions of ten seconds each, which give the DAQ's maximum allowed response during saturation.

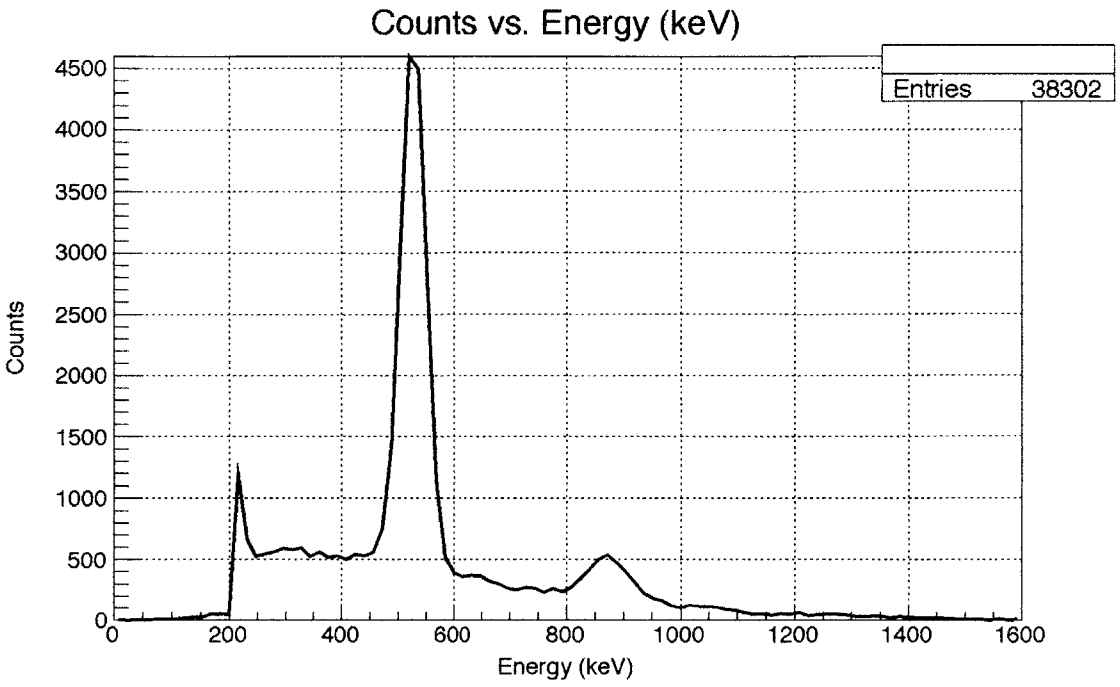

Figure 3.5: Maximum DAQ Response During Saturation, 10 seconds (1).

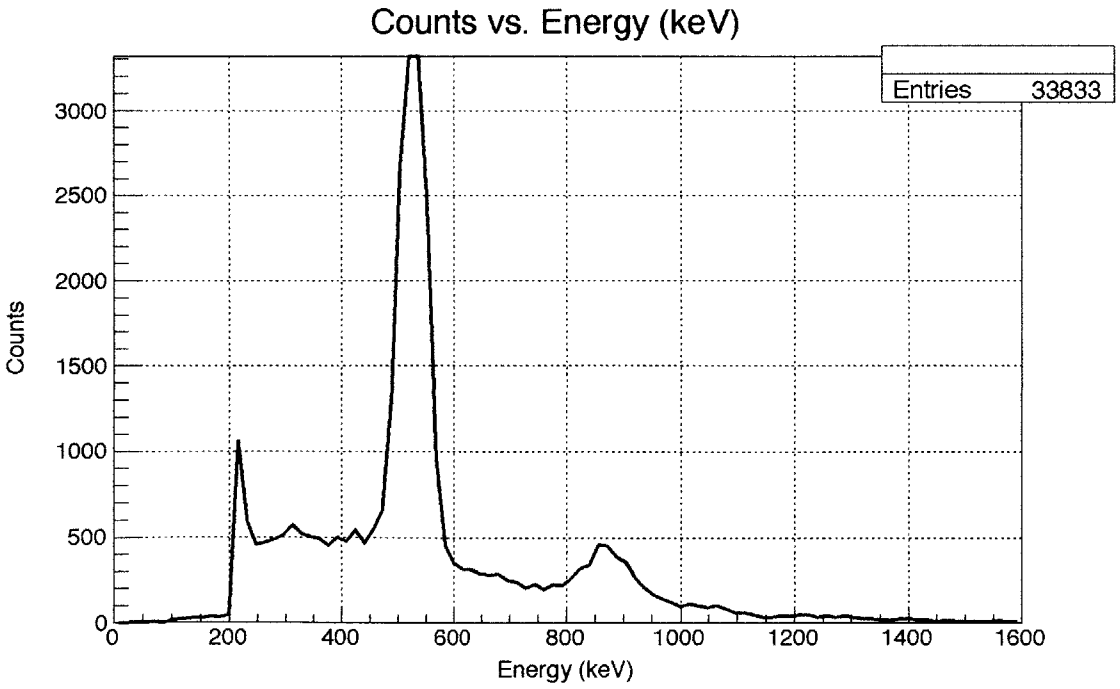

Figure 3.6: Maximum DAQ Response During Saturation, 10 seconds (2).

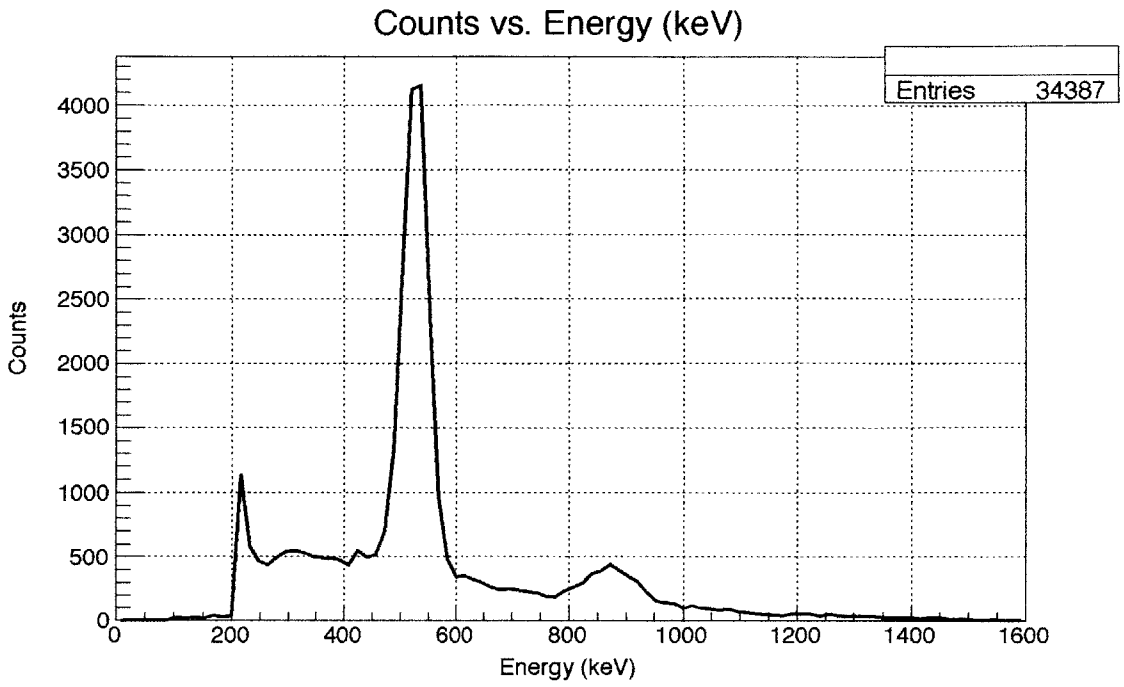

Figure 3.7: Maximum DAQ Response During Saturation, 10 seconds (3).

Thus, the DAQ system under "high-rate acquisition" mode and utilizing coincidence counting has a threshold of approximately 3500 counts per second. This design parameter should be taken into account when designing experimental geometry using the DAQ system. It should be noted here that this threshold exists in "pulse area spectrum" mode. Since integration of the pulse areas occurs during collection, this provides some of the slowdown in the system. Pulse height spectrum mode could provide some additional computational speed.

If the user wishes to use normal acquisition mode, there exists a DAQ response function in terms of spectrum refresh rate. This response function is calculated for various refresh rates and plotted against the maximum acquisition rate under high-rate

mode. The overall results are presented in Figure 3.8 in terms of maximum allowable counts per second.

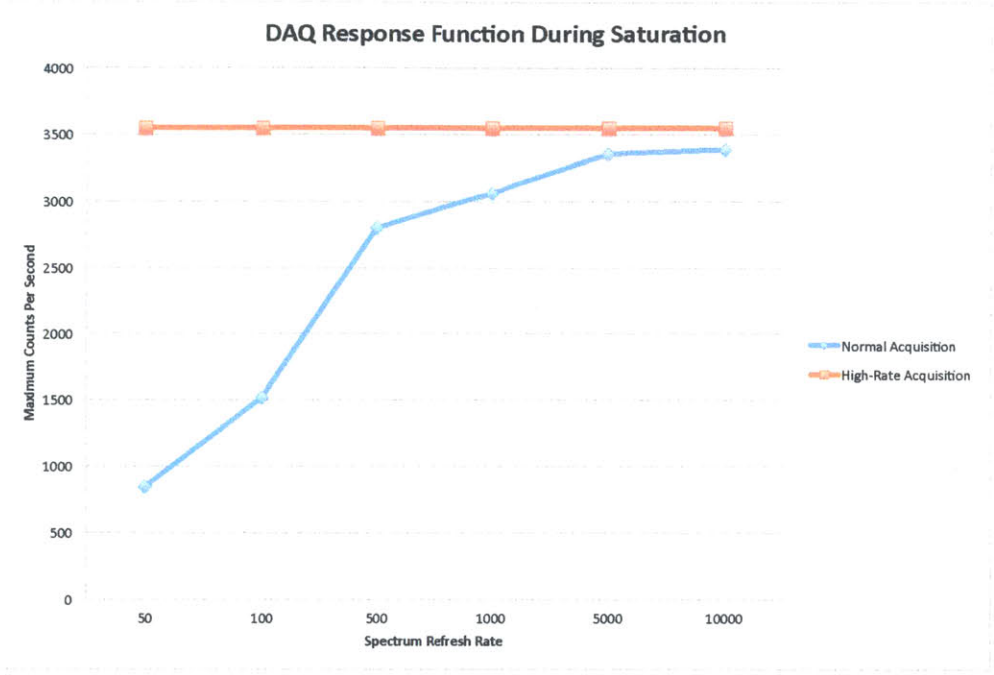

Figure 3.8: DAQ Response Function During Saturation.

From these results, one can see that normal acquisition approaches the limits of high-rate acquisition count rates at refresh rates of 5000 events. When comparing high-rate acquisition to normal acquisition, the DAQ software only slows down by a factor of approximately 5% at refresh rates of 5000 or 10000.

Experiment Limitations

The experimental setting at MGH was extremely useful in characterizing the USIC DAQ system, but some restrictions limited my ability to completely characterize the system for multiple geometries and levels of activity. Future work should seek to mitigate these limitations. First, the GE PETtrace cyclotron, as an industrial solution for large-scale radionuclide production, operates at energies and currents well beyond that of the design criteria of the USIC. For example, MGH's PETtrace operates at a fixed energy of 16 MeV for protons and a minimum current of 2 μA. Even 5 μA of protons on water for 5 minutes gives an output activity of 27 mCi. Due to the extremely high intrinsic efficiency of the 4" x 4" x 4" NaI detector and the limitations of the DAQ software, I was only able to calculate extremely low activities, often waiting for a number of half-lives in order to record coincident 511 keV gammas from the Nitrogen-13 sample. An experiment that employs an extremely small solid angle and shielding may allow one to conduct experiments at high activities, but there are some tradeoffs, including increased Compton scattering.

The second major limitation is that of the detectors themselves. As mentioned above, a 4" NaI cube has an extremely high intrinsic efficiency for 511 keV gammas; that is, a high ratio of the gammas that enter the detector cube at that energy interact with the detector, induce scintillation, and provide a response in the DAQ system. Future work might optimize the type of detector used. For example, according to Figure 3.3, a 2" NaI cube could provide robust calculations for activity levels two orders of magnitude greater

than a 4" cube, and a $LaBr_3$ detector could provide robust calculations for activity levels six orders of magnitude greater than the detectors in my array. An experimental setup with $LaBr_3$ detectors might provide activity calculations in the hundreds of milliCuries, which is a level of activity easily produced and often requested in a clinical setting. Indeed, normal cyclotron runs at MGH to produce Nitrogen-13 for quality control and for actual study typically yield approximately 300 mCi of activity from a 20 μA run for 15 minutes beam on target.[14]

Error Propagation

The confidence with which a patient is administered a radiopharmaceutical dose is extremely important. Thus, the concept of error propagation as it pertains to our detection scheme is of utmost importance.

I calculate error according to the following method. For any equation such as $z = xy$, the error is calculated as follows:

$$\frac{\partial z}{z} = \sqrt{(\frac{\partial x}{x})^2 + (\frac{\partial y}{y})^2} \tag{3.4}$$

My detector array consists of two 4" x 4" x 4" NaI detectors, each having an intrinsic efficiency of 0.44 with an error or uncertainty of approximately 10%. If we measure the activity of the sample in absolute terms, from Equation 3.1, in general, we

can expect to obtain an error of +/- approximately 16.5%, assuming we can measure the source-to-detector distance within 2 cm and the acquisition time within one second. Additionally, we take the error in the number of counts to be the square root of the number of counts, assuming Poisson statistics.

If we calculate the activity of the Nitrogen-13 sample using the relative method, however, we can obtain an error of +/- 11%, because the main source of error is the error in the activity of the known source. For the check source I used in my experiment, this was 10%. For a more expensive calibrated source, this error is roughly 5%. According to Massachusetts General Hospital, an error of approximately 10% is acceptable for patient administration.[15] Thus, for our purposes, the relative activity method is preferred. It is strongly recommended that IONETIX invest in a calibrated source with an error in activity of 5% in order to lessen error in future calculations.

ACTIVE INTERROGATION:

THE ^{11}B (d,nγ) ^{12}C REACTION

In 1968, Tepel et. al provided a study of the mechanism of the ^{11}B (d,nγ) ^{12}C reaction in terms of angular correlation. They conclude that this reaction is ideal for the production of monoenergetic gammas for two reasons. First, lower excited states of Carbon-12 are well-separated; and second, the gamma spectrum of the candidate reaction is simple, "since the competing (d,p) process only contributes to the low-energy region of the spectrum (Q(d,p) = 1.14 MeV) and most of the excited states of Carbon-12 decay by means of alpha-particle emission."[16] Figure 4.1 shows the ^{11}B (d,nγ) ^{12}C reaction scheme.

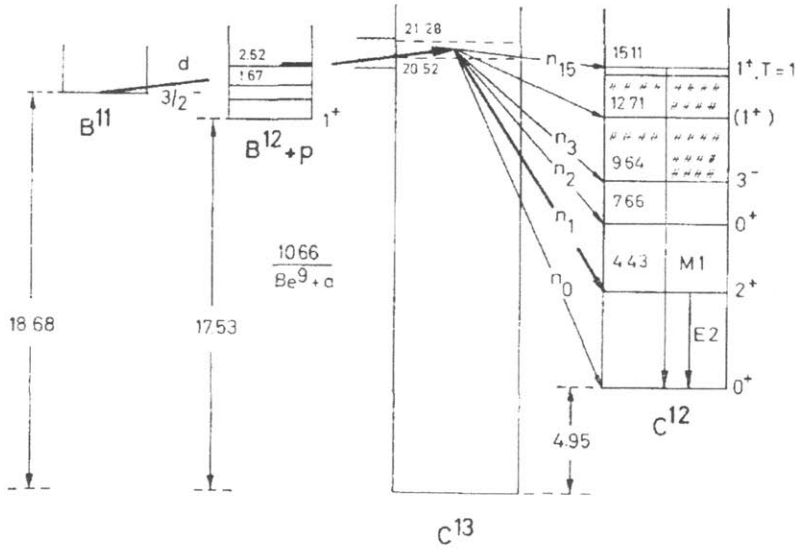

Figure 4.1: Level scheme of the ^{11}B (d,nγ) ^{12}C reaction.[17]

The production of monoenergetic gamma rays is essential for photofission processes that would be necessary for active interrogation of SNM which seek to capitalize on this reaction property. In 1984, Ries et. al measured the absolute photofission cross-sections for both Uranium-235 and Uranium-238, comparing their results to previous experiments. It is extremely useful that the ^{11}B (d,nγ) ^{12}C reaction produces 15.1 MeV gamma rays, as this is close to the peak photofission cross sections for both ^{235}U and ^{238}U.

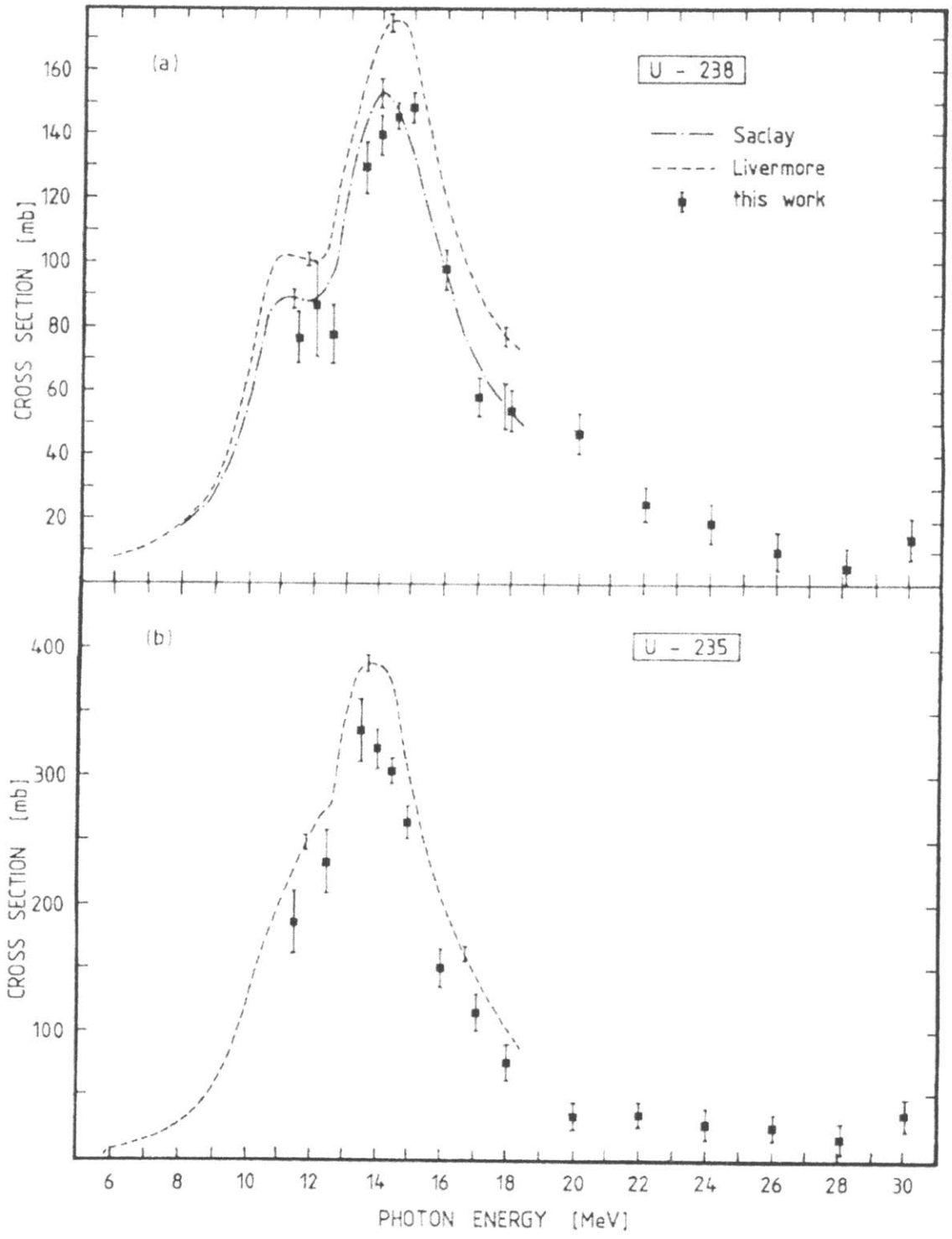

Figure 4.2: Experimental cross section $\sigma(\gamma,F)$ for ^{238}U (a) and ^{235}U (b). The dashed lines are smooth curves through the Saclay and Livermore data.[18]

In 2007, Morse et. al cite advantages and disadvantages related to both passive and active interrogation of nuclear material. Passive detection is problematic because natural decay signatures, especially of HEU, can be easily shielded. Active interrogation is advantageous because induced fission in a sample that contains nuclear material will have both photon and neutron sources, making shielding more difficult for a proliferator.[19] A potential drawback for active interrogation is dose to workers and others in the detection area. Additionally, the authors cite the utilization of a compact accelerator as particularly promising for active interrogation methods.

In 2011, Brandis et. al established a framework for active cargo inspection in order to detect both SNM (special nuclear material) and explosives. The legal requirements set forth by Public Law 110-53 (August 2007) mandated that within five years, all maritime and aviation cargo must be inspected for both SNM and explosives while in foreign port, prior to loading. Thus, many small systems capable of performing such detection must be readily available to deploy both within the US and in foreign ports of embarkation. Brandis et. al make use of the ^{11}B (d,nγ) ^{12}C reaction in order to maximize the utility of the Dual Discrete-Energy γ-Radiography (DDER) method. This reaction's "γ-spectrum is dominated by two well-separated γ-rays at 15.11 and 4.43 MeV. These give rise to an image contrast sensitivity (CS) for high-Z materials which is about a factor of 5 higher than that achievable with Dual-Energy Bremsstrahlung at electron energies of 5 and 9 MeV."[20] This allows for the detection of small quantities of SNM with a high degree of confidence. The candidate ^{11}B (d,nγ) ^{12}C reaction is also suitable for Fast Neutron Resonance Radiography (FNRR) which allows for the detection of explosives. Thus, a

system that incorporates the dual detection technologies of FNRR and DDER is ideally suited for cargo and port applications. Figure 4.3 shows a schematic of a FNRR/DDER system.

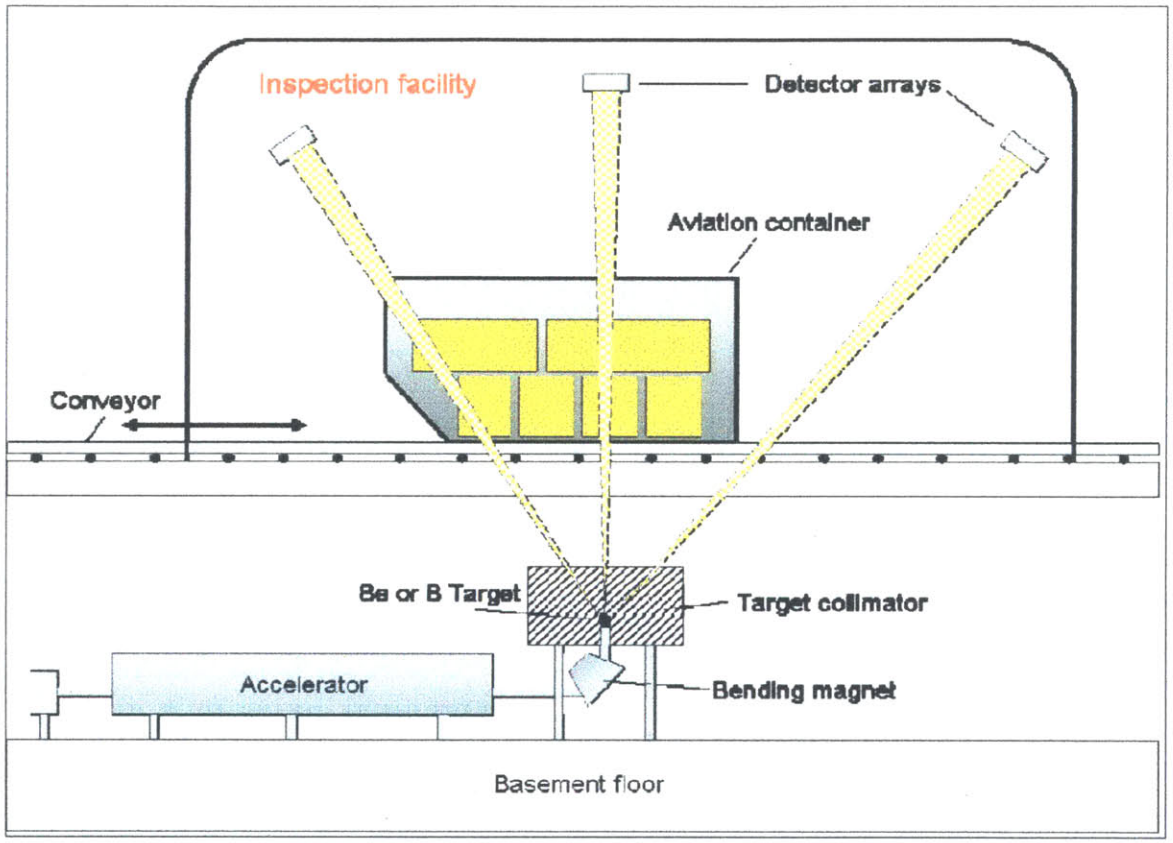

Figure 4.3: Schematic of a Combined FNRR/DDER System.[21]

A compact superconducting cyclotron is ideally suited for the accelerator portion of this detection system for two main reasons. First, the USIC can produce deuteron beam energies in the 5-7 MeV range, which is ideally suited for this application. According to Brandis's results, at these beam energies the production rate of the 4.43 MeV and the 15.1 MeV γ-rays are comparable. These results are show in Figure 4.4.

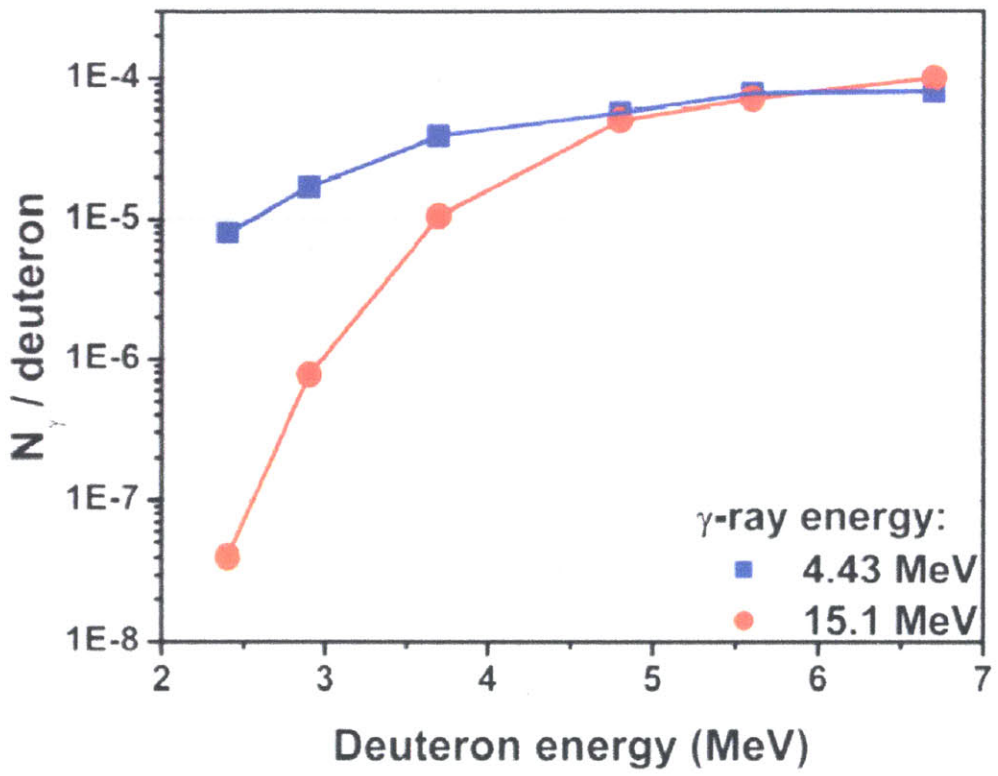

Figure 4.4: Measured γ-ray Yields as a Function of Deuteron Energy.[22]

Second, the USIC is mobile, and can be deployed or surged as needed if intelligence dictates an imminent threat. The "wall plug" feature of the USIC makes it extremely versatile and gives homeland security officials flexibility in designing detection schemes. The USIC has a smaller footprint and can be forklifted into place, as opposed to larger cyclotrons that require the infrastructure of entire rooms in order to operate.

My experiments with activity measurements of Nitrogen-13 have demonstrated a proof of concept for the USIC DAQ system. When the USIC generates reliable ion beam, the user must take care to set up experiment geometry so that the DAQ system

does not become saturated. With the DAQ as configured, extremely robust cross-section calculations for the ^{11}B (d,nγ) ^{12}C reaction are possible.

CONCLUSION

This thesis work summarizes many months of planning and coordination in order to characterize and comment on an important component of the IONETIX USIC system. The data acquisition system that I tested will allow the USIC project to go forward, and will demonstrate as a "proof of concept" that a compact cyclotron with a superconducting magnet could be used in both a clinical setting and in an active interrogation role.

This thesis work demonstrated two major findings. First, the production rates described by existing models accurately predict actual production rates in a cyclotron target. Experiment #1 demonstrated the DAQ's ability to calculate both absolute and relative activity. My findings indicate that relative activity calculations are both more accurate and precise. My major recommendation for future work on this project is that IONETIX acquire a positron check source with an activity with as small a calibration error as possible. This will allow relative activity calculations to be even more precise, which could be a major selling point in a clinical setting.

The second major finding of this thesis work is that there exists a saturation point for the DAQ system when utilizing the coincidence triggering feature, as is necessary when measuring the activity of a positron emitter such as Nitrogen-13. The saturation threshold value of 3500 counts per second should be taken into consideration when designing the USIC's initial testing. I recommend that the USIC run at currents on the order of nanoamps in order to ensure that output activity is kept low enough to detect

coincident 511 keV gammas without necessitating detector shielding. As the IONETIX team increases beam current to achieve clinical-level activity production, I recommend using 2" cube NaI detectors or a $LaBr_3$ detectors in order to take advantage of lower intrinsic efficiency. Combing detector choice with the experimental geometry will allow the team to conduct measurements at higher activities, while keeping the count rate below the threshold of 3500 counts per second.

In conclusion, I have demonstrated that characterization and performance assessment of the USIC utilizing our DAQ system is possible. I was able to validate a production rate model for Nitrogen-13 and offer recommendations for continued assessment and measurements moving forward.

REFERENCES

[1] Wells, P., R. J. A. Harte, and P. Price. "Positron Emission Tomography: A New Investigational Area for Cancer Research." Clinical Oncology 8.1 (1996): 7-14. Web. 24 June 2012.

[2] Antaya, T.A. "Introduction to Cyclotron Science and Technology; Lecture 2: There Are Three Kinds of Cyclotrons." *MIT Class Notes*.

[3] Ibid.

[4] E. Marshall, M.S. Thesis, *New Considerations for Compact Cyclotrons*, Massachusetts Institute of Technology (2012).

[5] Ibid.

[6] R. Kumar, H. Singh, M. Jacob, S. P. Anand, G. P. Bandopadhyaya, *Hellenic Journal of Nuclear Medicine* **12**, 248 (2009).

[7] Ibid.

[8] IAEA, "Nitrogen-13" in *Cyclotron Produced Radionuclides: Physical Characteristics and Production Methods*, Ed. Vienna (2009). p. 199.

[9] IAEA, "^{16}O (p,α) ^{13}N" in *Charged Particle Cross-Section Database for Medical Radioisotope Production: Diagnostic Radioisotopes and Monitor Reactions*, Ed. Vienna (2001), p. 245.

[10] Ibid., 243.

[11] Ibid., 244.

[12] IAEA, "^{16}O (p,α) ^{13}N".

[13] Hartwig Z. "Validation of Simulated Detector Efficiency." MIT 2012.

[14] R. Moore, Assistant Physicist, Massachusetts General Hospital Division of Nuclear Medicine and Molecular Imaging. Personal Communication. 22 Jan 13.

[15] J. Correia, Chief Physicist, Massachusetts General Hospital Division of Nuclear Medicine and Molecular Imaging. Personal Communication. 23 Apr 13.

[16] J. W. Tepel, M. Cosack, R. Felst, B. Zeitnitz, *Nuclear Physics A* **113**, 332 (1968).

[17] Ibid.

[18] H. Ries *et al.*, *Physical Review C* **29**, 2346 (1984).

[19] D. H. Morse, A. J. Antolak, B. L. Doyle, *Nuclear Instruments and Methods in Physics Research Section B: Beam Interactions with Materials and Atoms* **261**, 378 (2007).

[20] M. Brandis *et al.*, **AIP Conference Proceedings 1336**, 711 (2011).

[21] Ibid.

[22] ibid.

APPENDIX A

```
%   Shawn Fitzgerald

%   Cyclotron Data Acquisition Script
%   Absolute Activity Calculation for Nitrogen-13

%   15 Jan 2013

%   This script will read in data from the cyclotron's CyDAQRootGUI
%   program and perform the following functions:
%   1) plot the data in an energy spectrum, or histogram
%   2) calculate the activity of an unknown sample of Nitrogen-13
%   via both absolute and relative methods (relative method preferred)
%   3) calculate error in activity

clear

%   Ask the user if he/she wants to use absolute or relative activity

ans = input('Enter 1 for absolute activity, 2 for relative activity: ');

if ans == 1

%   Load the Background Data File into two vectors

%   Query the user for the Background data file name

[backName,backPath] = uigetfile('*', 'Select background file','.');
if backPath==0, error('None selected'); end
data_bg = load(fullfile(backPath,backName));

% data_bg = load('%bnd_file%.dat');      % loads the Background Data File
energy_bg = data_bg(:,1);          % places the energy bin along the x-axis
counts_bg = data_bg(:,2);          % places the counts along the y-axis

%   Load the Acquisition Data File into two vectors

[fileName,filePath] = uigetfile('*', 'Select data acquisition file','. );
if filePath==0, error('None selected'); end
data = load( fullfile(filePath,fileName) );
% data = load('spec1.dat');       % loads the Acquisition Data File
energy = data(:,1);             % places the energy bin along the x-axis
counts = data(:,2);             % places the counts along the y-axis

%   Generate error statistics for each count (assume Poisson statistics)

counts_bg_std = counts_bg .^ 0.5;   % finds stddev for background
counts_std = counts .^ 0.5;         % finds stddev for acquisition

counts_bg_minus = counts_bg - counts_bg_std;
counts_bg_plus = counts_bg + counts_bg_std;

counts_minus = counts - counts_std;
counts_plus = counts + counts_std;
```

```
%   Generate histogram or spectrum over the entire range

figure;
plot(energy,counts,'-');            % plots energy vs counts histogram
title('Counts vs. Energy');         % sets the title of the plot
xlabel('Energy (keV)');             % sets the label for the x-axis
ylabel('Counts');                   % sets the label for the y-axis
print -deps spectrum.eps            % prints to EPS file

%   Perform operations on the histogram

%   Get the user's region of interest to analyze

ROI_i = input('Enter the lower limit of the region of interest (keV): ');
ROI_f = input('Enter the upper limit of the region of interest (keV):  );

% if ROI_f <= ROI_i
%
%     fprintf('That range does not work, please re-enter')
%
% end

%   Parse the data according to the user's ROI

B = counts(find(energy >= ROI_i & energy <= ROI_f));
B_en = energy(find(energy >= ROI_i & energy <= ROI_f));

%   Get the applicable background from the user's ROI

C = counts_bg(find(energy_bg >= ROI_i & energy_bg <= ROI_f));
C_en = energy_bg(find(energy_bg >= ROI_i & energy_bg <= ROI_f));

%   Do error statistics on the ROI

B_std = B .^ 0.5;
B_std_minus = B - B_std;
B_std_plus = B + B_std;

C_std = C .^ 0.5;
C_std_minus = C - C_std;
C_std_plus = C + C_std;

%   Plot just the ROI

figure;
plot(B_en,B,'-',B_en,B_std_minus,'o',B_en,B_std_plus,'o');
% plots energy vs counts histogram
title('ROI Counts vs. Energy');         % sets the title of the plot
xlabel('Energy (keV)');                 % sets the label for the x-axis
ylabel('Counts');                       % sets the label for the y-axis
print -deps ROI.eps                     % prints to EPS file

%   Sum the total counts in the ROI

sum = cumsum(B);            % this gives the "total" activity
bck = cumsum(C);            % this gives the activity due to background
```

```
end_sum = sum(end);
end_bck = bck(end);

final = end_sum - end_bck;        % gives the "net" activity


%   Now I need to incorporate efficiency into this thing

%   Get the acquisition time from the user

t = input('What was the acquisition time, in seconds? ');

%   Get the decay fraction of the isotope in question from the user

f = input('What is the decay fraction of the isotope in question? ');

%   Get the intrinsic peak efficiency from the user
%   Assume 4x4x4 crystal size - assume 0.5

p = input('What is the intrinsic peak efficiency? ');

%   Calculate the geometric efficiency
%   Assume area of the detector is 16 cm^2 (4x4)

area = input('What is the area of the detector, in cm^2? ');
s = input('What is the source-to-detector distance, in cm? ');

g = area / (4 * pi * (s^2));

%   Now is when we can finally calculate the total activity of the sample

Bq = (final / t) * (1 / (g * p * f));  % Gives activity in Bq

Ci = Bq * 2.7*10^-11;                % Gives activity in Ci

uCi = Ci * 10^6   ;                        % Gives activity in uCi

%   Display the results

fprintf('The activity of the sample is:')

Bq

Ci

uCi

elseif ans == 2  % this begins the relative measurement loop

    %   Tell the user what to expect from the code

    i1 = input('Now we will do relative activity calculations: <Press Enter>');
    i2 = input('I need some info about the known sample of Na-22. <Press Enter>');


    %   Prompt the user for the known Na-22 spectrum (histogram) file
```

```
    ent1 = input('Press enter to select the known spectrum.');

    [knowName,knowPath] = uigetfile('*', 'Select known spectrum file','.');

    if knowPath==0, error('None selected!'); end
data_know = load( fullfile(knowPath,knowName) );  % loads the data file
know_energy = data_know(:,1);            % places the energy bin along the x-axis
know_counts = data_know(:,2);            % places the counts along the y-axis

%   We need to now figure out the activity of the known sample now, given
%   its calibration and time since calibration (in months)

stale = input('How many months has it been since known sample calibration? ');

mean_life = 31.2 * 1.4427;  % this is the mean half-life equation, Na-22 has a
                            % half-life of 31.2 months

fprintf('What was the activity of the source when calibrated?');
act_0 = input('Enter your answer in microCuries [uCi]: ');  % common unit of activity

ratio = exp( - stale / mean_life )          % calculates the ratio of activity, present to calib
act = act_0 * exp( - stale / mean_life )    % calculates the present activity of the calibrated

%   Get error in the "known" activity (assume 5%?)

fprintf('What is the error in the calibration of your known sample? );
fprintf('Enter your answer as a decimal, for example: ');
err_act = input('If there is 5% error, you would enter ".05": ');

%   Get acquisition time of the known spectrum

known_min = input('What was the known spectrum acquisition time, in minutes?  );
known_sec = known_min * 60;
known_hr = known_min / 60;

%   Prompt the user for the unknown spectrum (histogram) file

ent = input('Press enter to select the unknown acquisition spectrum.');

    [unkName,unkPath] = uigetfile('*', 'Select data acquisition file','.');

    if unkPath==0, error('None selected!'); end
data_unk = load( fullfile(unkPath,unkName) );
unk_energy = data_unk(:,1);            % places the energy bin along the x-axis
unk_counts = data_unk(:,2);            % places the counts along the y-axis

%   Get acquisition time of the unknown spectrum

unk_min = input('What was the unknown spectrum acquisition time, in minutes? );
unk_sec = unk_min * 60;
unk_hr = unk_min / 60;

%   Prompt the user for the background spectrum (histogram) file
```

```
ent3 = input('Press enter to select the background spectrum.');

    [bName,bPath] = uigetfile('*', 'Select background spectrum file','. );

    if bPath==0, error('None selected!'); end
rel_back = load( fullfile(knowPath,knowName) );
b_energy = rel_back(:,1);            % places the energy bin along the x-axis
b_counts = rel_back(:,2);            % places the counts along the y-axis

%   Get acquisition time of the background spectrum

back_min = input( 'What was the background acquisition time, in minutes? ');
back_sec = back_min * 60;
back_hr = back_min / 60;

%   Plot both the known and unknown spectra, and one figure with both
%   spectra

figure;
plot(know_energy,know_counts, '-');       % plots energy vs counts histogram
title('Calibration Counts vs. Energy');         % sets the title of the plot
xlabel('Energy (keV)');             % sets the label for the x-axis
ylabel('Counts');                   % sets the label for the y-axis
print -deps calibration.eps            % prints to EPS file

figure;
plot(unk_energy,unk_counts, '-');       % plots energy vs counts histogram
title('Unknown Counts vs. Energy');         % sets the title of the plot
xlabel('Energy (keV)');             % sets the label for the x-axis
ylabel('Counts');                   % sets the label for the y-axis
print -deps unknown.eps            % prints to EPS file

figure;
plot(know_energy,know_counts, '-',unk_energy,unk_counts,'-');
title('Calibration Counts vs. Energy');         % sets the title of the plot
xlabel('Energy (keV)');             % sets the label for the x-axis
ylabel('Counts');                   % sets the label for the y-axis
print -deps combo.eps            % prints to EPS file

%   Get the user's region of interest (ROI) to analyze

ROI_i = input('Enter the lower limit of the region of interest (keV): ');
ROI_f = input('Enter the upper limit of the region of interest (keV): ');

%   Parse the data according to the user's ROI

%   This is the array of counts for the known Na-22 spectrum within the ROI
Bknow = know_counts(find(know_energy >= ROI_i & know_energy <= ROI_f));

%   This is the array of counts for the unknown spectrum within the ROI
Bunk = unk_counts(find(know_energy >= ROI_i & know_energy <= ROI_f));

%   This is the array of energy values for the known Na-22 spectrum within the ROI
B_k = know_energy(find(know_energy >= ROI_i & know_energy <= ROI_f));

%   This is the array of energy values for the unknown spectrum within the ROI
```

```
B_u = unk_energy(find(unk_energy >= ROI_i & unk_energy <= ROI_f));

%   Get the applicable background from the user's ROI

%   This is the array of counts for the background within the ROI
C_temp = b_counts(find(b_energy >= ROI_i & b_energy <= ROI_f));

%   This is the array of energy values for the background within the ROI
C_en = b_energy(find(b_energy >= ROI_i & b_energy <= ROI_f));

%   Scale the background counts to match acquisition time of known/unknown
C = C_temp .* (unk_min / back_min);

%   Sum the counts

B_know_cum = cumsum(Bknow);      %   cumulatively sum the known Na-22 counts
B_unk_cum = cumsum(Bunk);        %   cumulatively sum the unknown counts
C_cum = cumsum(C);               %   cumulatively sum the background counts

end_unk = B_unk_cum(end);        %   takes the total counts within the ROI for the known Na-22 a
end_know = B_know_cum(end);      %   takes the total counts within the ROI for the unknown sampl
end_bck = C_cum(end);            %   takes the total counts within the ROI for the background

%   Calculate the activity of the unknown sample

%   Calculates the activity in microCuries
calculated_activity_uCi = act * ((end_unk - end_bck) / (end_know - end_bck));

%   Calculates the activity in milliCuries
calculated_activity_mCi = calculated_activity_uCi / 1000;

%   Calculate error

%   Calculate error in the counts (assume Poisson statistics)

err_known = Bknow .^ 0.5;    %   creates an array of error for known counts
err_unk = Bunk .^ 0.5;       %   creates an array of error for unknown counts
err_back = C .^ 0.5;         %   creates an array of errors for background

cum_err_known = cumsum(err_known);  %   cumulatively sums the known error array
cum_err_unk = cumsum(err_unk);      %   cumulatively sums the unknown error array
cum_err_back = cumsum(err_back);    %   cumulatively sums the background error array

end_err_known = cum_err_known(end);      %   total known count error
end_err_unk = cum_err_unk(end);          %   total unknown count error
end_err_back = cum_err_back(end);        %   total background count error

%   Make the error propagation calculation

num = (end_unk - end_bck);       %   numerator
den = (end_know - end_bck);      %   denominator
err_num = end_err_unk + end_err_back;    %   error in the numerator
err_den = end_err_known + end_err_back;  %   error in the denominator

frac = ((end_unk - end_bck) / (end_know - end_bck));    % "ratio" calcuation
```

```
err_frac = frac * (((err_num/num)^2 + (err_den/den)^2)^0.5);    %   error in the "ratio"

error_uCi = frac * err_act + err_frac * act;    %   calculates error in the
                                                %   uCi calcuation

error_mCi = error_uCi / 1000;                   %   calculates error in the
                                                %   mCi calcuation

%   Report the results

enter_final = input('Press enter to get your results!');

calculated_activity_uCi
error_uCi
calculated_activity_mCi
error_mCi

%   This is the last loop, and it terminates the program

else

    fprintf('You did not enter a proper entry. Goodbye.');

end


Error using input
Cannot call INPUT from EVALC.

Error in CyDAQAnalysisnocomm (line 19)
ans = input('Enter 1 for absolute activity, 2 for relative activity: ');
```

Published with MATLAB® 7.14